Synth. Commun. **1992**, *22*, 214.
10. Karabatsos, G. J.; Hsi, N. *Tetrahedron* **1967**, *23*, 1079.
11. (a) Knorr, R.; Weiss, A.; Low, P.; Rapple, E. *Chem. Ber.* **1980**, *113*, 2462; (b) Montgomery, F. C.; Saunders, Jr., W. H. *J. Org. Chem.* **1976**, *41*, 2368; (c) Knorr, R. *Chem. Ber.* **1980**, *113*, 2441; (d) Smith, J. K.; Bergbreiter, D. E.; Newcomb, M. *J. Am. Chem. Soc.* **1983**, *105*, 4396; (e) Guthrie, R. D.; Burdon, L. G.; Lovell, Jr. F. L. *J. Org. Chem.* **1973**, *38*, 3114.
12. MTPA=α-Methoxy-α-(trifluoromethyl)phenylacetic acid: Brown, H. C.; Kim, K-W.; Cole, T. E.; Singaram, B. *J. Am. Chem. Soc.* **1986**, *108*, 6761.
13. Brown, H. C.; Kramer, G. W.; Levy, A. B.; Midland, M. M. *Organic Synthesis via Organoboranes*; Wliley Interscience: New York, 1975; chapter 9.

Revised Reversible and Totally Irreversible Zones for the Linear Sweep Voltammetry at a Planar Electrode

Juhyoun Kwak*

**Department of Chemistry, Korea Advanced Institute of Science and Technology, Taejon 305-701*

Received September 1, 1993

Digital simulation program for one-dimensional geometric systems of electrochemical phenomena was developed. The accuracy of the digital simulation is discussed by comparing with the known solutions. Applying this program to the linear sweep voltammetry at a planar electrode for the electrode reaction, O+ne→R, the accurate current functions for the reversible and totally irreversible charge transfer systems were obtained. Comparing these current functions with the simulated voltammograms for various other values of α (0.1 to 1.0) and Λ (10^{-5} to 10^{5}), the revised zones that are different from those proposed by Matsuda and Ayabe for the reversible and totally irreversible systems are proposed. For α≥0.1, the reversible zone is in $\Lambda \geq 10^{1.7}$ and the totally irreversible zone is in $\Lambda \leq 10^{-1.7}$, where $\Lambda = k^{\circ}/[D_o^{1-\alpha} D_R^{\alpha} (nF/RT)v]^{1/2}$.

Introduction

The Fick's first law of flux and the mass conservation law, instead of the differential equations of the Fick's second law, can be easily implanted into a computer code to obtain the dynamic currents for complex electrochemical phenomena in any geometries. This method is called as the digital simulation[1] that should be distinguished from the numerical calculation to solve the integro-differential equations or the serial form of analytical solutions. Except a few cases of electrochemical diffusion problem[2], the analytical solutions for the differential equations representing the Fick's second law cannot be obtained with ease. Even the analytical solution is available, it might be the serial form of integral functions like Bessel functions[3], so that the tedious numerical calculation hinders the access to the accurate real numerical values. Then, digital simulation method is preferred because of detouring the mathematical complexity as well as less computer calculation time. To decrease the simulation time but not to sacrifice the accuracy, the various techniques were developed. Among them, the exponentially expanding space grid[4,5] and the Crank-Nicholson method[1,6] were employed in this work. In the simulation of chronoamperometry, the exponentially expanding time grid was also employed successfully.

In this report, the simplest electrode reaction, O+ne→R, at a planar electrode is considered to focus on the accuracy of the simulation. This will provides firm base to leap into the more complex problems, for example, the complex electrode reactions at the various geometric systems of planar, spherical, cylindrical, disk, multiple bands, and ring electrode systems. Primarily, the accuracy of the simulation was checked by comparing with the analytical solution of diffusion controlled chronoamperometric currents, *i.e.*, Cottrell equation, at a planar electrode. In case of linear sweep voltammetry, assuming the true peak current can be obtained by the infinite number of space grids and potential step grids, the true peak current can be obtained by extrapolating the bilinearly changing peak current values depending on the square of the space grid size and the square of the potential step size. Secondarily, the current functions of the reversible and totally irreversible systems for the linear sweep voltammetry at a planar electrode were also compared with that of Nicholson and Shain[7] or Suzuki[8]. Since the current functions of this work are believed to be more accurate, the revised tables of these functions are presented. Finally, the voltammograms for various values of α (0.1 to 1.0) and Λ (10^{-5} to 10^{5}) are obtained to compare with these two current functions. The voltammogram of specific value of α and Λ is compared with those of above tabulated functions. If the deviations from the current function of the reversible system or that of the totally irreversible system in all the simulated potential range are same in 1% error range, then that α and Λ value is included in the reversible system or the totally irreversible system. In this way, two distinctive zones are obtained as $\Lambda \geq 10^{1.7}$ for the reversible system and Λ $10^{-1.7}$ for the totally irreversible system. These are different from those proposed by Matsuda and Ayabe[9], where Λ≥15

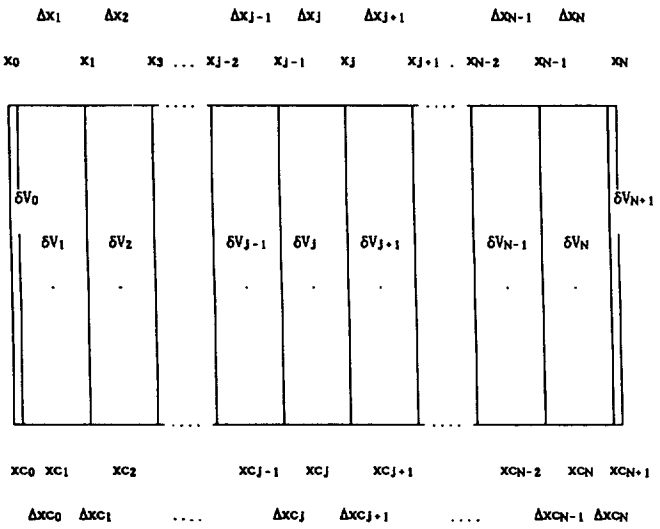

Figure 1. Space grid indexing.

for the reversible system and $\Lambda \leq 10^{-2(1+\alpha)}$ for the totally irreversible system.

Method

Review of Fick's laws. Fick's first law[2] states that the flux of species i in fluid state is proportional to the concentration gradient of species i. But, Fick's first law cannot be used to explain the migrational effect, *i.e.*, the flux of ionic species by the electrical field. The more general statement of flux law, which satisfies Fick's first law and considers migration and convection, is that the flux of species i in fluid state is proportional to the impressed force[10]. But, in this work, the first statement was employed for the simple situation where the migrational effect is negligible, the activity coefficients of all electroactive species are 1, and the convection of fluid is negligible.

For the symbolic representation of Fick's first law, the clearly defined notations of the space and time grid are useful. Especially, the space grid indexing as shown in Figure 1 is critical for the computer coding of nonlinear space grid as described later. The x_{j-1} is for the location of left plane of box δV_j. The x_j is for the location of right plane of box δV_j. The difference between x_j and x_{j-1} is defined as Δx_j. This is a typical gridding found in many monographs[1,11]. Here, x_0 is the location of electrode surface and x_N can be the semi-infinite distance from the electrode or the location of another electrode in thin layer cell system. In this work, it is thought that the clearly defined extra indexing symbols are not harmful for the simplicity of digital simulation. That is xc_j which represents the center location in box δV_j, *i.e.*, $xc_j=(x_j+x_{j-1})/2$. For the future purpose, xc_0 is considered as a center of volume element (δV_0) of negligible size at the electrode surface. Similarly, xc_{N+1} is considered as a center of volume element (δV_{N+1}) of negligible size. Because of of negligible volume size, $xc_0=x_0$ and $xc_{N+1}=x_N$. Note that xc_{N+1} is not same as xc_N. Similar time gridding was used, *i.e.*, t_k $(k=0,1,\cdots,L)$, Δt_k $(k=1,2,\cdots,L)$, tc_k $(k=0,1,\cdots,L+1)$, and Δtc_k $(k=0,1,\cdots,L)$ where t_0 is the initial time and t_L is the final time.

In digital simulation, the average currents (*i.e.*, heterogeneous electron transfer rates) at an electrode surface in given time intervals and the average concentrations of all electroactive species in discretized volumes δV_j $(j=1,2,\cdots,N)$ are aimed to be solved instead of the analytical current function of t and the continuous concentration function of x and t.

From Fick's first law, the flux of species i through a plane of unit area at a location x_j at a time t_k, symbolized as $J_i(x_j, t_k)$, can be approximated as follows.

$$J_i(x_j, t_k) = -D_i[\underline{C}_i(xc_{j+1}, t_k) - \underline{C}_i(xc_j, t_k)]/\Delta xc_j \quad (1)$$

where D_i is the diffusion coefficient of species i and the $\underline{C}_i(xc_j, t_{k-1})$ is the average concentration of species i in δV_j. The above equation is simply a finite difference form of the well-known equation,

$$J_i(x, t) = -D_i\, dC_i(x, t)/dx \quad (2)$$

The schemes in which the average flux of species i through a plane at x_j during t_k and t_{k+1}, symbolized as $\underline{J}_i(x_j, t_k/t_{k+1})$, is assumed to be same as $J_i(x_j, t_k)$,

$$\underline{J}_i(x_j, t_k/t_{k+1}) = -D_i[\underline{C}_i(xc_{j+1}, t_k) - \underline{C}_i(xc_j, t_k)]/\Delta xc_j \quad (3)$$

are called fully explicit or the FTSC representation (forward time centered space)[12]. In other words, in an explicit method, only the concentrations of old time t_k are used to represent the average flux between old time t_k and new time t_{k+1}. On the other hand, in a fully implicit method, only the concentrations of new time t_{k+1} are used as follows.

$$\underline{J}_i(x_j, t_k/t_{k+1}) = -D_i[\underline{C}_i(xc_{j+1}, t_{k+1}) - \underline{C}_i(xc_j, t_{k+1})]/\Delta xc_j \quad (4)$$

While a fully implicit method is stable for arbitrarily large timesteps, a fully explicit method is stable only for sufficiently small timesteps. In general, $\underline{J}_i(x_j, t_k/t_{k+1})$ can be approximated by mixing these two methods, *i.e.*,

$$\underline{J}_i(x_j, t_k/t_{k+1}) = (1-\theta)\, J_i(x_j, t_k) + \theta\, J_i(x_j, t_{k+1}) \quad (5)$$

where $0 \leq \theta \leq 1$. The methods using $\theta = 1/2$ and $2/3$ are respectively called as the Crank-Nicholson method and the Galerkin method. Both methods are still unconditionally stable[6,12]. In this work, the Crank-Nicholson method is used throughout all the digital simulation for the stability and the accuracy[12].

The Fick's second law can be easily understood from the consideration of the number of species i in δV_j ($\delta V_j = A\ \Delta x_j$ and A is the side area of a box).

(Change of Number of species i in δV_j for time interval between t_k and t_{k+1})

$$= \underline{C}_i(xc_j, t_{k+1})\ \delta V_j - \underline{C}_i(xc_j, t_k)\ \delta V_j$$

$$= -(\text{outflux of species } i \text{ to right side during } t_k \text{ and } t_{k+1}) + (\text{influx of species } i \text{ from left side during } t_k \text{ and } t_{k+1})$$

$$= -\underline{J}_i(x_j, t_k/t_{k+1})\ A\ \Delta t_k + \underline{J}_i(x_{j-1}, t_k/t_{k+1})\ A\ \Delta t_k \quad (6)$$

Dividing by δV_j,

$$C(xc_j, t_k) - C(xc_j, t_{k-1}) = -[\underline{J}_i(x_j, t_k/t_{k+1}) - \underline{J}_i(x_{j-1}, t_k/t_{k+1})]\Delta t_k/\Delta x_j \quad (7)$$

or

$$[C(xc_j,\ t_k)-C(xc_j,\ t_{k-1})]/\Delta t_k= -[J_i(x_j,\ t_k/t_{k-1})-J_i(x_{j-1},\ t_k/t_{k-1})]/\Delta x_j \quad (8)$$

The combined equation of (1) and (8) is a finite difference form of the well-known differential equation for Fick's second law, *i.e.*,

$$dC_i(x,\ t)/dt=-dJ_i(x,\ t)/dx=D_i\ (d^2C_i(x,\ t)/dx^2). \quad (9)$$

Among the above equations, only three simple and elementary Eqs. (1), (5), and (7) are used in digital simulation instead of a final differential Eq. (9) itself. The similar discussion for heat conduction problem is well described in the physics textbook[13]. The difference is that, in mass transfer case, the concentrations of multiple species are to be solved instead of one physical variable, *i.e.*, temperature. More importantly, the boundary condition is distinctively different.

Boundary Flux. The flux of species i at x_j ($j=1,2,\cdots, N-1$) can be solved by Eq. (1) described as above. The fluxes at x_N can be considered as zero when the concentrations in δV_N is not perturbed by letting x_N as semi-infinite distance away[2], $x_N=10\ (D_F\ t_L)^{1/2}$ in this work, from the electrode surface where the perturbation begins. Here D_F means the largest diffusion coefficient among those of all electroactive species. Then, one thing left to be formulated is boundary flux[11] at the electrode surface. Considering the electrode reaction, O+ne→R, the oxidized species (O) near the electrode surface obtains n electrons in the rate of $k_f\ \underline{C}_O(xc_0,\ t_k)$ from the chemically inert and conducting electrode to become other species (R). Likewise, backward reaction, R −ne→O, is occurred at the electrode surface at the rate of $k_b\ \underline{C}_R(x_0,\ t_k)$. Since the oxidized species is disappeared by forward reaction and generated by backward reaction,

$$J_O(x_0,\ t_k)=-k_f(t_k)\ \underline{C}_O(xc_0,\ t_k)+k_b(t_k)\ \underline{C}_R(x_0,\ t_k) \quad (10)$$

Apparently, the fluxes of the electro-inactive species are zero simply because the mass flow is blocked. In a simple redox reaction which is considered in this work, only two electroactive species (O and R) change their oxidation states and their fluxes at the electrode surface can be nonzero by heterogeneous reaction. But, since the chemical species cannot actually disappear into the electrode surface though the oxidation states of species are changed, total flux of chemical species at the electrode surface, $J_o(x_0,\ t_k)+J_R(x_0,\ t_k)$, should be zero. This is the flux balance equation.

$$J_o(x_0,\ t_k)=-J_R(x_0,\ t_k) \quad (11)$$

Since the negative flux (flux toward the electrode) of oxidized species is caused by the flux of electron from the electrode surface, the current flow through the electrode is

$$I=-nFAJ_o(x_0,\ t_k) \quad (12)$$

where n electrons per an oxidized species are needed.

Though the $J_o(x_0,\ t_k)$ and $J_R(x_0,\ t_k)$ are caused by the heterogeneous electron transfer, the mass transfers between the center of δV_1 and δV_0 are restricted by Fick's first law, *i.e.*,

$$J_o(x_0,\ t_k)=-D_o[\underline{C}_o(xc_1,\ t_k)-\underline{C}_o(xc_0,\ t_k)]/\Delta xc_0 \quad (13)$$

$$J_R(x_0,\ t_k)=-D_R[\underline{C}_R(xc_1,\ t_k)-\underline{C}_R(xc_0,\ t_k)]/\Delta xc_0 \quad (14)$$

From (10), (13), and (14),

$$\underline{C}_o(xc_0,\ t_k)=\underline{C}_o(xc_1,\ t_k)+J_o(x_0,\ t_k)\Delta xc_0/D_R \quad (15)$$

$$\underline{C}_R(xc_0,\ t_k)=\underline{C}_R(xc_1,\ t_k)-J_o(x_0,\ t_k)\Delta xc_0/D_R \quad (16)$$

From (15) and (16), Eq. (10) becomes

$$J_o(x_0,\ t_k)=-k_f(t_k)\ [\underline{C}_o(xc_1,\ t_k)+J_o(x_0,\ t_k)\Delta xc_0/D_R] +k_b(t_k)\ [\underline{C}_R(xc_1,\ t_k)-J_o(x_0,\ t_k)\Delta xc_0/D_R] \quad (17)$$

Rearranging (17),

$$J_o(x_0,\ t_k)=[-k_f(t_k)\ \underline{C}_o(xc_1,\ t_k)+k_b(t_k)\ \underline{C}_R(xc_1,\ t_k)] /[1+k_f(t_k)\Delta xc_0/D_R+k_b(t_k)\Delta xc_0/D_R] \quad (18)$$

Here, the heterogeneous kinetic constants $k_f(t_k)$ and $k_b(t_k)$ are functions of electrode potential, $E(t_k)$, which changes linearly in the linear sweep voltammetry. For the relationship between kinetic constants and electrode potential, Butler-Volmer[2] kinetic model was used in this work.

$$k_f(t_k)=k^\circ\ \exp[-\alpha(nF/RT)\ (E(t_k)-E^{\circ\prime})] \quad (19)$$

$$k_b(t_k)=k^\circ\ \exp[(1-\alpha)(nF/RT)\ (E(t_k)-E^{\circ\prime})] \quad (20)$$

where α is called the transfer coefficient, k° is the intrinsic heterogeneous kinetic constant, and $E^{\circ\prime}$ is the formal potential for O+ne→R. From (18) along with (19) and (20), the boundary flux at the electrode surface can be solved.

Matrix equation. From (1), (5), (7) and (18), the concentrations at t_{k+1} can be solved by the concentrations at t_k. For the fully explicit method, the resulting matrix equation as shown below is easy to solve because the matrix inversion process is not necessary. A 2N×2N matrix $\boldsymbol{D}(t_k)$ is a 5 band diagonal matrix and a function of known variables, D_o, D_R, $k_f(t_k)$, Δxc_j, and Δt_k.

$$\begin{Bmatrix} \underline{C}_o(xc_1,\ t_{k+1}) \\ \underline{C}_R(xc_1,\ t_{k+1}) \\ \underline{C}_o(xc_2,\ t_{k+1}) \\ \underline{C}_R(xc_2,\ t_{k+1}) \\ \cdot \\ \cdot \\ \cdot \\ \underline{C}_o(xc_N,\ t_{k+1}) \\ \underline{C}_R(xc_N,\ t_{k+1}) \end{Bmatrix} = \begin{bmatrix} \\ \\ \\ \\ \\ \boldsymbol{D}(t_k) \\ \\ \\ \\ \\ \end{bmatrix} \cdot \begin{Bmatrix} \underline{C}_o(xc_1,\ t_k) \\ \underline{C}_R(xc_1,\ t_k) \\ \underline{C}_o(xc_2,\ t_k) \\ \underline{C}_R(xc_2,\ t_k) \\ \cdot \\ \cdot \\ \cdot \\ \underline{C}_o(xc_N,\ t_k) \\ \underline{C}_R(xc_N,\ t_k) \end{Bmatrix} \quad (21)$$

or briefly

$$\underline{\boldsymbol{C}}(t_{k+1})=\boldsymbol{D}(t_k)\ \underline{\boldsymbol{C}}(t_k) \quad (22)$$

But, in the Crank-Nicholson method, the resulting matrix equation

$$\boldsymbol{D}(t_{k+1})\ \underline{\boldsymbol{C}}(t_{k+1})=\boldsymbol{D}(t_k)\ \underline{\boldsymbol{C}}(t_k) \quad (23)$$

has a matrix at the left hand side, so the matrix inversion process is necessary. Again, $\boldsymbol{D}(t_k)$, and $\boldsymbol{D}(t_{k+1})$ are 5 band diagonal matrixes and functions of known variables, D_o, D_R, $k_f(t_k)$, $k_b(t_k)$, $k_f(t_{k+1})$, $k_b(t_{k+1})$, Δxc_j, and Δt_k. The efficient matrix inversion routine[12] in C-language was used. The computer code for Eq. (23) is constructed by C-language and compiled by Turbo-C 3.0. Once $\underline{\boldsymbol{C}}(t_{k+1})$ (concentrations at t_{k+1}) is solved, then the average flux and current during t_k and t_{k+1} can be calculated by Eq. (5) and (12).

Exponentially expanding grid. The exponential algo-

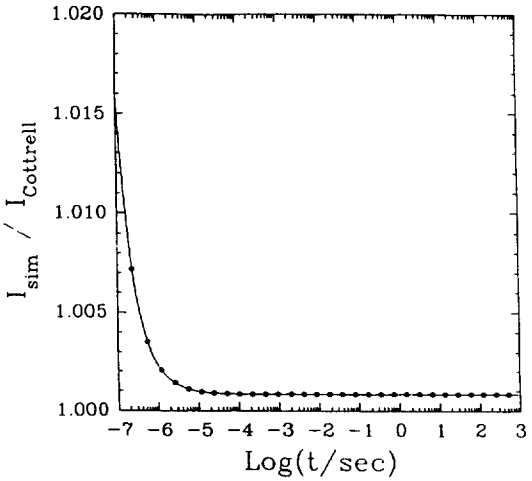

Figure 2. Digital simulation error in chronoamperometry.

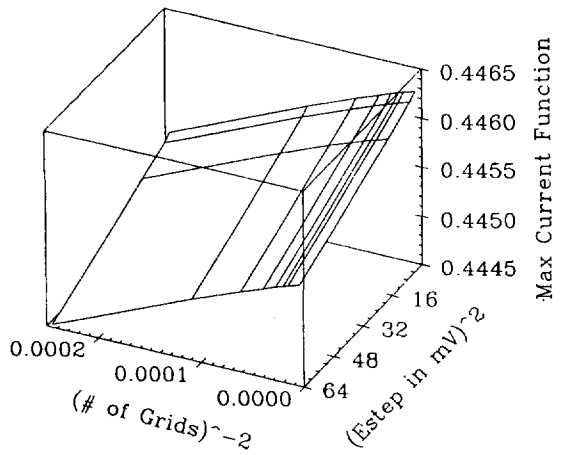

Figure 3. Digital simulation error in the linear sweep voltammetry of reversible charge transfer system.

rithm which was developed by Joslin and Pletcher[4] and refined by Feldberg[5] was employed to generate the nonlinear space and time grids, *i.e.*,

$$\Delta x_j = \Delta x_1 \exp[\beta(j-1)] \tag{24}$$

or

$$x_j = \Delta x_1 [\exp(\beta j)-1]/[\exp(\beta)-1] \tag{25}$$

But, in this work, the method was modified to vary the number of grids, not the exponential factor β. From the nonlinear Eq. (25), β was solved by given values of Δx_1, x_N, and N. Once β is solved, Δx_j ($j=2,3,\cdots,N$), x_j ($j=1,2\cdots,N-1$), $xc_j=(x_j+x_{j-1})/2$ ($j=1,2,\cdots,N$), and $\Delta xc_j=xc_{j-1}-xc_j (j=0,1,\cdots,N)$ can be solved immediately. In this way, the nonlinear space grid can be explicitly defined by only three input variables, *i.e.*, Δx_1, x_N, and N. Similarly, the nonlinear time grid also can be explicitly defined by Δt_1, t_L, and L.

Results and Discussion

Error analysis of chronoamperometry. Using the C-language program based on the previous section, a diffusion controlled chronoamperometric curve was simulated and compared with the Cottrell equation. The simulation variables in MKS units were $D_o=D_R=10^{-9}$ m^2/sec, $\Delta x_1=5\times10^{-9}$ m, $x_N=1\times10^{-2}$ m, $N=128$, $\Delta t_1=1.25\times10^{-8}$ sec, $t_L=1\times10^3$ sec, $L=128$, $E-E^{\circ\prime}=-1.0$ V, $k^\circ=10^8$ m/sec, $C_o^*=1$ mol/m^3, $C_R^*=0$ mol/m^3, $n=1$, and $T=298.15$ K, where C_i^* is the bulk concentration of species i. Note that $DM=D_o\Delta t_1/(\Delta x_1)^2 \le 0.5$. The relative errors versus time are shown in Figure 2. In a wide range of time (10^{-5} sec to 10^3 sec), the error is less than 0.08%. Considering that the execution time was 13 sec in 486-DX PC computer, it is proved that the nonlinear gridding method which is employed in this work is very efficient and accurate.

Current function of the reversible system. Using the same program, the linear sweep voltammetric response was simulated by the linearly changing electrode potential with the scan rate υ. But, instead of nonlinear time grid, the linear time grid (therefore the linear electrode potential grid) was used in this case. Not like the Cottrell equation for the chronoamperometry, the analytical solution for the linear sweep voltammetry is integral form[7,8] which should be numerically solved and usually represented by the numerical table form.

For the discussion of general quasi-reversible kinetics, the dimensionless kinetic parameter[9] $\Lambda=k^\circ/[D_o^{1-\alpha}D_R^{\alpha}(nF/RT)\upsilon]^{1/2}$ and the current function[9] $\Psi=1/[nFAC^*D_o^{1/2}(\upsilon nF/RT)^{1/2}]$ are employed. The reversible and totally irreversible systems are the limiting cases of the general quasi-reversible system. If k° (or Λ') approaches to infinite, the term on the left-hand side of Eq. (10) is negligible compared to the individual terms on the right side. From Eqs. (10), (19), and (20), the Nernst equation for the reversible system is resulted, $C_o(xc_0, t_k)/C_R(x_0, t_k)=\exp[(nF/RT)(E(t_k)-E^{\circ\prime})]$. To simulate the reversible system, a new program based on the Dirichlet boundary condition[12] can be constructed. In this work, simply a huge number, 10^{12}, was used for Λ in the general quasi-reversible kinetics system program. It can be increased more as long as the numerical value can be accepted by the computer program and does not lead to out-of-range number during the computation. The value, 10^{12}, is more than enough considering that even smaller $\Lambda=10^3$ well describes the reversible system[9]. This value can be handled without difficulty in the double precision program which allows the value upto 1.7×10^{308}.

To check the accuracy of the simulated result, it is accepted as a true statement that the simulated result approaches to a true peak current value by increasing the grid number and the potential grid to infinite number. The peak values of the simulated current function Ψ_{sim} are shown in Figure 3. It turns out to be that the digital error is bilinear to the inverse square of the number of space grid and the square of the potential step size. The asymptotic value of the peak value of current function Ψ (or $\sqrt{\pi}\chi(at)$), 0.44630, is the accepted true value. By this accepted true value, the digital error is 0.004% for $N=512$ and $\Delta E=1$ mV. Therefore, upto 5 digits of the current function values which are tabulated in Table 1 are believed to be significant.

Current function of totally irreversible system. Exactly same strategy as used in the case of reversible system was used to obtain the current function of the totally irreversible system, using $\alpha=0.5$ and $\Lambda=10^{-4}$. The corrected current function[7,9] Ψ_{corr} ($\Psi_{corr}=\Psi/\sqrt{\alpha}=\sqrt{\pi}\chi(bt)$) versus

Table 1. Current function ($\Psi=\sqrt{\pi}\chi(at)$) values for reversible charge transfer

$n(E-E_{1/2})$, mV	Current function values		
	Ref. 7	Ref. 8	This work
120	0.009	0.0091	0.00925
100	0.020	0.0197	0.01983
80	0.042	0.0416	0.04180
60	0.084	0.0847	0.08496
50	0.117	0.1180	0.11833
45	0.138	0.1382	0.13849
40	0.160	0.1607	0.16100
35	0.185	0.1855	0.18576
30	0.211	0.2122	0.21251
25	0.240	0.2405	0.24081
20	0.269	0.2698	0.27007
15	0.298	0.2993	0.29952
10	0.328	0.3281	0.32829
5	0.355	0.3553	0.35544
0	0.380	0.3800	0.38007
−5	0.400	0.4013	0.40139
−10	0.418	0.4187	0.41880
−15	0.432	0.4319	0.43196
−20	0.441	0.4408	0.44076
−25	0.445	0.4453	0.44536
−28.5	0.4463	0.4463	0.44625
−30	0.446	0.4461	0.44610
−35	0.443	0.4435	0.44346
−40	0.438	0.4380	0.43800
−50	0.421	0.4210	0.42095
−60	0.399	0.3991	0.39916
−80	0.353	0.3528	0.35295
−100	0.312	0.3123	0.31242
−120	0.280	0.2800	0.28021
−150	0.245	0.2447	0.24487

Table 2. Corrected current function ($\Psi_{corr}=\Psi/\sqrt{\alpha}=\sqrt{\pi}\chi(bt)$) values for irreversible charge transfer

E_{corr}, mV	Corrected current function	
(see text)	Ref. 7	This work
160	0.003	0.00349
140	0.008	0.00756
120	0.016	0.01633
110	0.024	0.02391
100	0.035	0.03489
90	0.050	0.05062
80	0.073	0.07289
70	0.104	0.10377
60	0.145	0.14536
50	0.199	0.19906
40	0.264	0.26422
35	0.300	0.29993
30	0.337	0.33648
25	0.372	0.37256
20	0.406	0.40661
15	0.437	0.43695
10	0.462	0.46200
5	0.480	0.48051
0	0.492	0.49177
−5	0.496	0.49573
−5.34	0.4958	0.49575
−10	0.493	0.49300
−15	0.485	0.48469
−20	0.472	0.47220
−25	0.457	0.45695
−30	0.441	0.44020
−35	0.423	0.42294
−40	0.406	0.40591
−50	0.374	0.37411
−70	0.323	0.32293

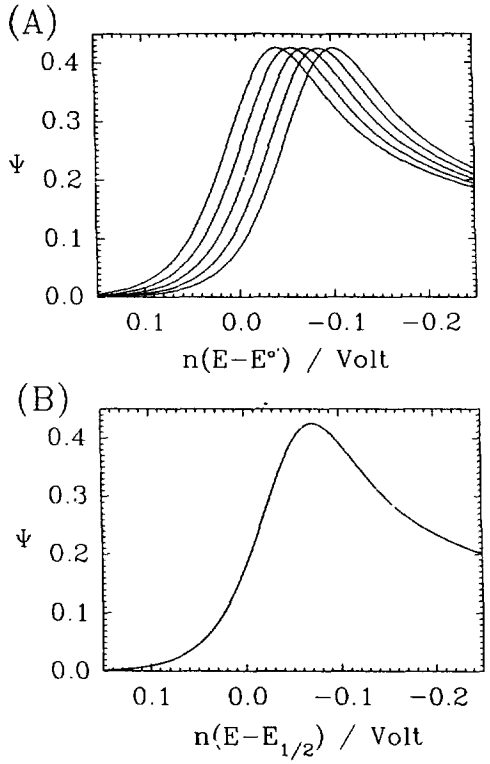

Figure 4. $\log(D_R/D_o)$ dependency of the linear sweep voltammetric curves for $\alpha=0.7$ and $\log\Lambda=-0.5$. (A) Ψ *vs* $n(E-E_{1/2})$; $\log(D_R/D_o)=1.0$, 0.5, 0, −0.5, and 1.0 from left to right. (B) Ψ *vs* $n(E-E_{1/2})$; 5 voltammograms of (A) are folded together. $E_{1/2}=E^{\circ\prime}+(RT/nF)\ln(D_R/D_o)^{1/2}$.

the corrected potential[7] E_{corr} ($E_{corr}=(E-E_{1/2})\alpha n+(RT/F)\ln((\pi D_o\alpha(nF/RT)\upsilon)^{1/2}/k^{\circ})$) is tabulated in Table 2. The accepted true value of peak Ψ_{corr} is 0.49580.

Potential shift by D_o/D_R[9]. In general, the potential of the current functions even for the quasi-reversible systems is shifted by the amount of $(RT/nF)\ln(D_R/D_o)^{1/2}$ as shown in Figure 4, Therefore, in Table 1 and 2, $E_{1/2}=E^{\circ\prime}+(RT/nF)\ln(D_R/D_o)^{1/2}$ was used instead of $E^{\circ\prime}$ for general case of $D_o/D_R\neq1$.

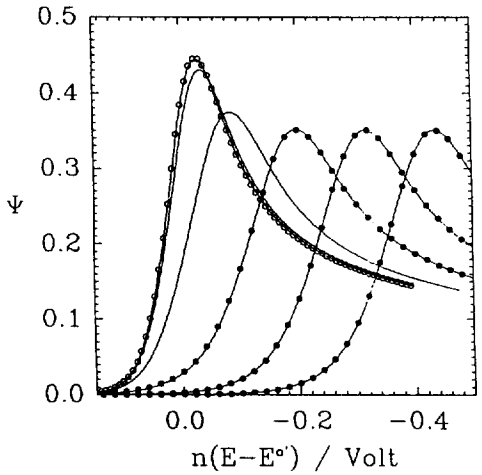

Figure 5. Linear sweep voltammetric curves for $\alpha=0.5$. Solid lines (—); digital simulation curve for log $\Lambda=1.5$, 0.5, −0.5, 1.5, 2.5, and 3.5 from left to right. Open circle (○); current function of reversible charge transfer system. Closed circle (●); current function of totally irreversible charge transfer system.

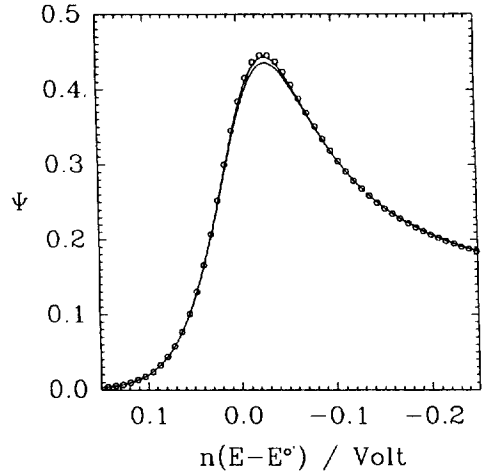

Figure 6. Linear sweep voltammetric curves for $\alpha=0.1$. Solid lines (—); digital simulation curve for log $\Lambda=1.7$ (upper) and 1.2 (lower). Open circle (○); current function of reversible charge transfer system.

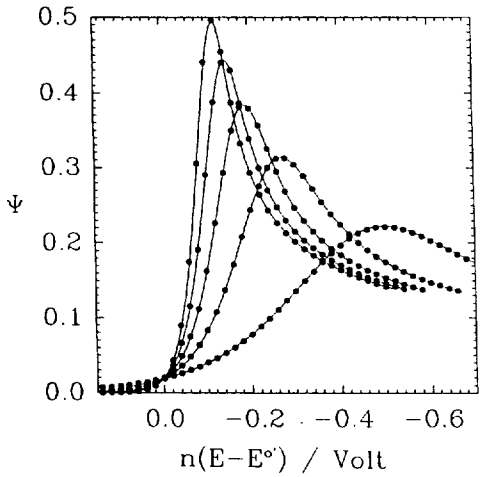

Figure 7. Linear sweep voltammetric curves for log $\Lambda=-1.7$. Solid lines (—); digital simulation curve for $\alpha=1.0$, 0.8, 0.6, 0.4, and 0.2 from left to right. Closed circle (●); current function of totally irreversible charge transfer system.

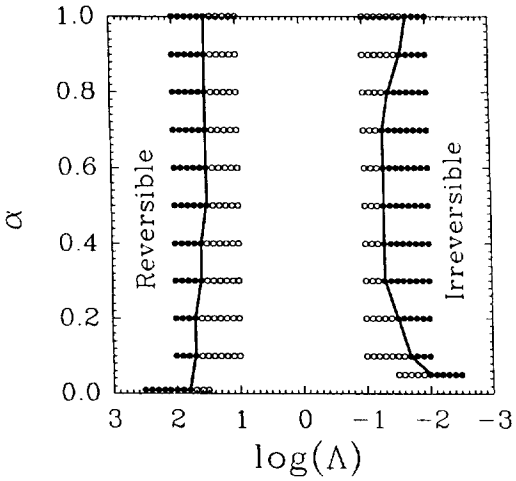

Figure 8. Zones of the reversible and totally irreversible systems for the linear sweep voltammetry at a planar electrode. Open circle (○); error of 1% over. Closed circle (●); error of 1% or less.

Zones for reversible and totally irreversible system. Since the accurate current functions of the reversible and totally irreversible systems are obtained, it is a matter of iteration to find whether the simulated voltammogram for various α and Λ is similar to one of this system or not. To reduce the time for the simulations of all possible case of α and Λ, the less sparse grid parameters, $N=128$ and $\Delta E=2$ mV, were used. For this gridding, in Figure 2, the error is 0.07% for the reversible systems and similarly 0.07% for the irreversible systems. Therefore, for the arbitrary α and Λ, the digital error is less than 0.07%. This error is more than enough to check whether the simulated voltammogram is deviated 1% from the tabulated current functions.

Typical voltammograms are shown in Figure 5, for $\alpha=0.5$ and various log $\Lambda=1.5$, 0.5, −0.5, 1.5, 2.5, and 3.5. For log $\Lambda=1.5$, it is exactly same as the reversible function (open circles). For log $\Lambda=1.5$, 2.5, and 3.5, those are exactly same as the irreversible current function (filled circle). But, log $\Lambda=0.5$ and −0.5, none of the tabulated current functions is not fitted. It is categorized as a quasi-reversible system. According to Matsuda and Ayabe[9], the reversible system is defined as $\Lambda\geq 15$ for any α. But, as shown in Figure 6, the simulated voltammogram for $\Lambda=10^{1.2}=15.85$ and $\alpha=0.1$, the deviation of peak current is 4%. In the criterion for this report, it is quasi-reversible.

Typical irreversible voltammograms for log $\Lambda=-1.7$ and various $\alpha=1.0$, 0.8, 0.6, 0.4, and 0.2, are shown in Figure 7. All the curves are same as the irreversible current function (filled circle). According to Matsuda and Ayabe, none of these cases is irreversible system (log $\Lambda\leq -2(1+\alpha)$). Inconsistency is evident because the larger error range (4% for over) is allowed for the reversible system, but the very

restricted error range (less than 1%) is allowed for the irreversible system. Therefore, the revised criterions have to be proposed in the practical point of view.

In Figure 8, the numerous voltammograms are checked to figure out the zones for the reversible system and the irreversible system for the linear sweep voltammetry. From this figure, it is proposed that for $1 \geq \alpha \geq 0.1$, the reversible zone is in $\Lambda \geq 10^{1.7}$ and the totally irreversible zone is in $\Lambda \leq 10^{-1.7}$.

Conclusion

The accurate and efficient digital simulation program for one-dimensional electrochemical phenomena was developed. It is demonstrated that the digital simulation program based on the combined algorithm of the Crank-Nicholson scheme and the exponentially expanding grids is very accurate and efficient for the simulation of chronoamperometry. Applying this to the linear sweep voltammetry at a planar electrode for the electrode reaction, $O + ne \rightarrow R$, the accurate current functions for the reversible and totally irreversible heterogeneous electron transfer systems were obtained. The voltammograms of all the range of α (0.1 to 1.0) and Λ (10^{-5} to 10^{5}) are compared with the current functions of the reversible system and the totally irreversible system. If the deviations from the current function of the reversible system or that of the totally irreversible system in all the simulated potential range are same in 1% error range, then that α and Λ value is included in the reversible system or the totally irreversible system. In this way, the values of α and Λ for the reversible system and the totally irreversible system are collected to find the zones. In result, the reversible zone is in $\Lambda \geq 10^{1.7}$ and the totally irreversible zone is in $\Lambda \leq 10^{-1.7}$ for $1 \geq \alpha \geq 0.1$.

Acknowledgement. This work was supported by the Korea Science and Engineering Foundation (Grant No. 923-0300-003-2).

References

1. Feldberg, S. W. In *Electroanalytical Chemistry*; Bard, A. J. Ed.; Marcel Dekker: New York, **1969**; Vol. 3.
2. Bard, A. J.; Faulkner, L. R. *Electrochemical Methods: Fundamentals and Applications*; John Wiley & Sons: New York, 1980, Chapter 5.
3. Wightman, R. M.; Wipf, D. O. In *Electroanalytical Chemistry*; Bard, A. J. Ed.; Marcel Dekker: New York, **1989**; Vol. 15.
4. Joslin, T.; Pletcher, D. *J. Electroanal. Chem.* **1974**, *49*, 171.
5. Feldberg, S. W. *J. Electroanal. Chem.* **1981**, *127*, 1.
6. Huebner, K.; Thornton, E. A. *The Finite Element Method for Engineers*; 2nd ed.; John Wiley & Sons: New York, 1982; p 293-297.
7. Nicholson, R. S.; Shain, I. *Anal. Chem.* **1964**, *36*, 706.
8. Suzuki, T.; Mori, I.; Nagamoto, H.; Ito, M. M.; Inoue, H. *J. Electroanal. Chem.* **1992**, *324*, 397.
9. Matsuda, H.; Ayabe, Y. *Z. Elektrochem.* **1955**, *59*, 494.
10. Atkins, P. W. *Physical Chemistry, 4th ed.;* Oxford University Press: Oxford, 1990; p 763.
11. Feldberg, S. W. In *Computers in Chemistry and Instrumentation*; Vol. 2, *Electrochemistry: Calculation, Simulation, and Instrumentation*; Mattson, J. S.; Mark, Jr., H. B.; MacDonald, Jr., H. C. Eds.; Marcel Dekker: New York, 1972.
12. Press, W. H.; Flannery, B. P.; Teukolsky, S. A.; Vetterling, W. T. *Numerical Recipes in C: The Art of Scientific Computing*; Cambridge University Press: Cambridge, 1988, Chapter 7.
13. Feynman, R. P.; Reighton, R. B.; Sands, M. *The Feynman Lectures on Physics*; Addison-Wesley, Reading: **1964**; Vol. II, Chapter 3.